Journal of Catalysis 257 (2008) 181–189

Contents lists available at ScienceDirect

Journal of Catalysis

www.elsevier.com/locate/jcat

Selective oxidation of propylene over model supported V_2O_5 catalysts: Influence of surface vanadia coverage and oxide support

Chunli Zhao, Israel E. Wachs *

Operando Molecular Spectroscopy and Catalysis Laboratory, Departments of Chemistry and Chemical Engineering, Lehigh University, Bethlehem, PA 18015, USA

ARTICLE INFO

Article history:
Received 4 March 2008
Revised 24 April 2008
Accepted 25 April 2008
Available online 27 May 2008

Keywords:
Catalyst
Supported vanadium oxide
ZrO_2, TiO_2, Nb_2O_5, Al_2O_3, SiO_2
Reaction
Selective oxidation
Propylene
Acrolein
In situ
Raman spectroscopy
FT-IR
UV–vis DRS

ABSTRACT

The selective oxidation of propylene to acrolein was investigated over well-defined supported vanadium oxide catalysts as a function of the oxide support (Al_2O_3, SiO_2, Nb_2O_5, TiO_2 and ZrO_2) and surface vanadia coverage in the sub-monolayer region (<8 V atoms/nm^2). The supported vanadia catalysts were synthesized by incipient wetness impregnation of vanadium isopropoxide/isopropanol solutions and subsequently dried and calcined at elevated temperatures to form the surface vanadia species. The molecular structures and oxidation states of the supported vanadia catalysts were examined with *in situ* UV–vis and Raman spectroscopy in different environments (oxidizing, reducing and during propylene oxidation reaction). The supported vanadia phase is found to be present as surface VO_4 species in the sub-monolayer region and becomes partially reduced during the propylene oxidation reaction environment. The propylene oxidation to acrolein TOF increases with surface vanadia coverage because two surface VO_4 sites are involved in the rate-determining-step for acrolein formation. At monolayer surface vanadia coverage, the acrolein TOF varies by a factor of $\sim 10^2$ as a function of the specific oxide support: $V_2O_5/ZrO_2 \sim V_2O_5/TiO_2 > V_2O_5/Nb_2O_5 > V_2O_5/Al_2O_3 > V_2O_5/SiO_2$. This reactivity trend inversely varies with the electronegativity of the oxide support cation, which controls the electron density on the bridging V–O–support bond and the availability of the bridging oxygen atom for redox reactions. This suggests that bridging V–O–support bond is the catalytic active site for the selective oxidation of propylene to acrolein.

1. Introduction

The selective oxidation of propylene over bulk Bi–Mo–O mixed metal oxides to acrolein (CH_2=CHCHO) and acrylic acid (CH_2=CHCOOH), chemical intermediates for the preparation of synthetic fibers and other valuable products, was initially developed during the 1960s [1–3]. There is now intense interest in developing similar catalytic technologies for acrolein and acrylic acid starting with less expensive propane. The catalysts found to be able to activate propane for these oxygenated products are vanadium-containing bulk mixed metal oxides such as vanadium pyrophosphate ($(VO)_2P_2O_7$), heteropoly acids and salts ($M_{1-x}PV_1M_xMo_{11-x}O_{40}$, M = Co^{2+}, Fe^{3+}, Ga^{3+}, Ni^{2+}, Sb^{3+} or Zn^{2+}), and multi-component mixed oxides of Mo–V–Te–Nb (Sb)–O [4–6]. The selective oxidation of propane to acrolein and acrylic acid proceeds via the following reaction network: propane → propylene → acrolein → acrylic acid [6]. The selective oxidation of propane to oxygenates, thus, critically depends on the efficiency of the propylene oxidation reaction step. The absence of systematic studies in the catalysis literature on selective propylene oxidation to oxygenates over vanadium-based metal oxide catalysts, especially model supported vanadia catalysts, prevents the establishment of molecular/electronic structure–activity/selectivity relationships for this critical catalytic reaction step.

Only several studies have reported on propylene oxidation to oxygenates over supported vanadia catalysts. Photo-oxidation of propylene with UV excitation over supported V_2O_5/SiO_2 was found to yield aldehyde (CH_3CHO, C_2H_5CHO, and CH_2=CHCHO) as the main reaction products [7]. Photo-excitation of propylene over mesoporous V_2O_5/FSM-16 yielded over 40% propylene oxide for short contact times and high conversion [8]. Propylene was found to be selectively oxidized to acetone over supported V_2O_5/TiO_2 catalysts in the presence of water vapor [9]. Acetone was also the major reaction product during propylene oxidation in the presence of water vapor over ultra stable Y-type zeolite catalysts [10]. The current authors recently reported that propylene is selectively oxidized to acrolein over supported V_2O_5/Nb_2O_5 catalysts [11]. The different supported vanadia catalysts and reaction conditions are most likely responsible for the various reaction products observed during propylene oxidation.

The objective of the present investigation is to examine the influence of the specific oxide support and surface vanadia coverage on the selective oxidation of propylene to oxygenates (primarily acrolein). Propylene oxidation was examined over well de-

* Corresponding author. Fax: +1 (610) 758 6555.
E-mail address: iew0@lehigh.edu (I.E. Wachs).

0021-9517/$ – see front matter
doi:10.1016/j.jcat.2008.04.022

fined model supported vanadia catalysts (V_2O_5/ZrO_2, V_2O_5/TiO_2, V_2O_5/Al_2O_3, V_2O_5/Nb_2O_5, and V_2O_5/SiO_2) where the catalytic active vanadia is exclusively present as two-dimensional surface vanadia species on the high surface area oxide supports. The molecular and electronic structures of the catalytic surface vanadia species were determined with *in situ* Raman spectroscopy and UV–vis diffuse reflectance spectroscopy (DRS), respectively. The corresponding catalytic activity and selectivity were chemically probed with the steady-state propylene oxidation reaction. The combination of the spectroscopic and catalytic performance data allows for the establishment of molecular/electronic structure–catalytic activity/selectivity relationships for propylene oxidation by supported vanadia catalysts.

2. Experimental

2.1. Catalyst synthesis

The supported V_2O_5 catalysts were prepared on Al_2O_3 (Engelhard, $S_{BET} = 203\ m^2/g$), ZrO_2 (Degussa, $S_{BET} = 39\ m^2/g$), TiO_2 (Degussa P-25, $S_{BET} = 45\ m^2/g$), Nb_2O_5 (CBMM, $S_{BET} = 59\ m^2/g$) and SiO_2 (Cabosil EH-5, $S_{BET} = 332\ m^2/g$) by the incipient-wetness impregnation method. The amount of the vanadium isopropoxide ($VO(O\text{-}^iPr)_3$ precursor (Alfa-Aesar, 97% purity), corresponding to the desired amount of vanadium oxide loading, and the 2-propanol solvent (Fisher ACS, 99.9% pure), corresponding to incipient wetness impregnation volume, were thoroughly mixed with the oxide support in a glove box under flowing N_2. After impregnation, the samples were initially dried in flowing N_2 at 120 °C for 1 h, further dried at 300 °C for an additional 1 h, and finally calcined in flowing air at 300 °C for 1 h and 450 °C for 2 h.

2.2. BET surface area

The BET surface area of the oxide supports was determined in order to calculate the vanadium surface density of the supported vanadium oxide catalysts. The BET surface area was measured by nitrogen adsorption/desorption isotherms employing a Quantasorb surface area analyzer (Quantachrome Corporation, Model OS-9) using a 3:7 ratio of a N_2/He mixture. Typically, 0.1–0.3 g of sample was used for the measurement and the sample was outgassed at 200 °C prior to N_2 adsorption at −195.8 °C.

2.3. In situ Raman spectroscopy

The *in situ* Raman spectra of the supported vanadia catalysts under dehydrated and propylene oxidation reaction conditions were obtained with the Horiba–Jobin Yvon LabRam-High Resolution Raman spectrometer system. The single stage monochromator system possesses a confocal microscope (Olympus BX-30), a notch filter (532 nm) and a 900 grooves/mm grating. The scattered photons were directed and focused onto a sensitive LN_2 CCD detector (JY-CCD3000). The *in situ* Raman spectra were collected in the 200–1800 cm^{-1} region with 532 nm excitation (Coherent 315, YAG doubled diode pumped laser, 20 mW). Typically, only 5–10 mg of the supported vanadia catalysts was placed into the *in situ* environmental cell (Linkman TS-1500) as loose powder. The *in situ* Raman spectra of the dehydrated catalysts were collected after heating the catalyst sample to 450 °C for 1 h in flowing 10% O_2/He (Scott Specialty Gases, O_2, 99.996% purity; He, ultrahigh purity) and cooling the sample down to room temperature.

The *in situ* Raman spectra during propylene oxidation at 300 °C were obtained in the 200–1800 cm^{-1} region employing the following protocol. The sample was initially heated at 450 °C for 1 h in a flowing 10% O_2/He mixture. The background Raman spectrum was taken after the sample was cooled to 300 °C. Different ratios of the 2.96% C_3H_6/He (Scott Specially Gases, C_3H_6, 99.996% purity; He, ultrahigh purity) and 10% O_2/He corresponding to 1:6, 1:1, 3:1 and 10% O_2/He were introduced into the environmental cell and the Raman spectra at 300 °C were collected after reaching steady-state (typically ∼30 min). The used catalysts were subsequently reoxidized in the flowing O_2/He mixture from 300 to 450 °C after the reaction, and the Raman spectra were again recorded of the reoxidized catalyst.

2.4. In situ UV–vis DRS

Ultraviolet–visible (UV–vis) diffuse reflectance spectroscopy (DRS) measurements of the supported vanadia catalysts were performed on a Varian Cary 5E UV–vis NIR spectrophotometer. The *in situ* UV–vis DRS spectra were taken in the 200–800 nm range with a Harrick DRS cell (HVC-DR2) under dehydrated and reaction conditions at 300 °C. The catalyst samples were loaded as loose powders into the environmental cell and the dehydrated MgO UV–vis DRS at 300 °C was used as the baseline reference for the supported vanadia catalysts.

The catalyst samples were initially pretreated at 400 °C in 10% O_2/He for 1 h and cooled to 300 °C to obtain the UV–vis DRS of the dehydrated samples. Propylene oxidation with varying C_3H_6/O_2 ratios (1:6, 1:1, 3:1 and ∞) were performed at 300 °C with a total flow rate of 50 cm^3/min. The UV–vis DRS spectra were further processed to obtain the Kubelka–Munk function ($F(R\infty)$) from the absorbance. The edge energy, Eg, for allowed transitions was determined by finding the intercept of the straight line in the low energy rise of a plot of $(F(R\infty) \times h\nu)^2$ against $h\nu$, where $h\nu$ is the incident photon energy [12,13].

2.5. Propylene oxidation catalytic studies

The steady-state catalytic experiments were carried out in a fixed-bed Pyrex glass tubular reactor (¼' OD and 1 ft long) connected to an online GC (Agilent 6890) equipped with a Supelco capillary column, which was connected to a FID detector in series with a Carboxene-1000 packed column connected to a TCD detector. A six-port valve with a 0.5 cm^3 loop was used for sampling of the gases exiting from the reactor.

The reactant gas flow rates of propylene, O_2, and He were adjusted through separate mass flow controllers (Brooks Model 5850E Series) to a total flow of 50 ml/min. The typical amount of catalyst employed was between 10 and 30 mg. The catalytic reaction was examined between 250 and 400 °C and the propylene conversion was maintained below 5% to ensure differential reaction conditions. The reactor system and the injection to the gas chromatograph were maintained in a vented hood because of the toxicity of the reaction products such as acrolein, acrylic acid and CO. The catalytic activity values were converted to turnover frequency (the number of acrolein molecules formed per V atom per second) since the catalytic active supported vanadia phase was 100% dispersed on the oxide supports (see Raman spectroscopy characterization in Section 3.2 below).

3. Results

3.1. BET surface area of supports and vanadia surface density on the supports

The BET surface area of the oxide supports (ZrO_2, TiO_2, Nb_2O_5, Al_2O_3 and SiO_2) and supported vanadia surface density (V/nm^2) values are given in Table 1. The surface vanadia surface density calculation assumes that the oxide support surface area is constant since surface vanadia has only a modest effect on the surface area of the support [14] and the supported vanadia phase is present as

Table 1
BET values of oxide supports and vanadia surface density (V/nm^2) for the supported vanadia catalysts

Catalysts	Support	Support S_{BET} (m^2/g)	Surface density (V atoms/nm^2)
1% V_2O_5/Al_2O_3	Al_2O_3	203	0.3
5% V_2O_5/Al_2O_3	(Engelhard)		1.7
10% V_2O_5/Al_2O_3			3.6
20% V_2O_5/Al_2O_3			8.2[a]
1% V_2O_5/ZrO_2	ZrO_2	39	2.0
2% V_2O_5/ZrO_2	(Degussa)		4.0
3% V_2O_5/ZrO_2			6.0
4% V_2O_5/ZrO_2			8.1[a]
1% V_2O_5/TiO_2	TiO_2	45	1.4
2% V_2O_5/TiO_2	(Degussa P-25)		3.0
3% V_2O_5/TiO_2			4.5
4% V_2O_5/TiO_2			6.1
5% V_2O_5/TiO_2			7.7
1% V_2O_5/Nb_2O_5	Nb_2O_5	59	1.1
3% V_2O_5/Nb_2O_5	(Niobium Products Co.)		3.5
5% V_2O_5/Nb_2O_5			5.9
7% V_2O_5/Nb_2O_5			8.4[a]
1% V_2O_5/SiO_2	SiO_2	332	0.2
5% V_2O_5/SiO_2	(Cabosil EH-5)		1.0
8% V_2O_5/SiO_2			1.7
10% V_2O_5/SiO_2			2.2
12% V_2O_5/SiO_2			2.7[b]

[a] Monolayer surface vanadia coverage.
[b] Highest loading without formation of crystalline V_2O_5 NPs.

a two-dimensional overlayer (see Section 3.2 below). Below monolayer surface coverage, the supported vanadia phase is ~100% dispersed on the oxide supports. Monolayer surface vanadia coverage corresponds to ~8 V/nm^2 on the oxide supports with the exception of SiO_2 where monolayer coverage cannot be attained because of the low reactivity of its surface hydroxyls [15–17].

3.2. *In situ* Raman spectroscopy

3.2.1. Dehydrated conditions (O_2/He at 300 °C)

Crystalline V_2O_5 nanoparticles (NPs), with the sharp characteristic V_2O_5 Raman band at ~995 cm^{-1}, are only detected above monolayer surface coverage (>8 V/nm^2) for the supported 4% V_2O_5/ZrO_2, 5% V_2O_5/TiO_2, 7% V_2O_5/Nb_2O_5, and 20% V_2O_5/Al_2O_3 catalysts [18]. The Raman spectra for the dehydrated supported vanadia catalysts with approximately monolayer surface coverage are shown in Figs. 1–3 under oxidizing conditions at 300 °C. The Raman spectrum of the supported 4% V_2O_5/ZrO_2 (8.1 V/nm^2) catalyst contains bands from the dehydrated surface VO_4 species at ~1035 and ~935 cm^{-1} arising from the terminal V=O and bridging V–O–Zr bonds, respectively [19]. The stronger Raman features at ~630, ~552, ~528, ~470, ~375, and ~330 cm^{-1} are from the crystalline ZrO_2 (monoclinic) support. Similar surface VO_4 vibrational bands at ~1035 and 935/900 cm^{-1} are also present in the Raman spectra of the dehydrated supported V_2O_5/Al_2O_3 and V_2O_5/TiO_2 catalysts, respectively (see Figs. 2 and 3 under O_2/He conditions). The TiO_2 support also exhibits strong Raman bands at ~393, ~505, and ~632 cm^{-1} and a weaker overtone band at ~790 cm^{-1} from the crystalline TiO_2 (anatase) phase [18]. The Al_2O_3 support does not give rise to Raman bands, which allows for the detection of additional surface vanadia vibrations at lower wavenumber values, and reveals the presence of bridging V–O–V bonds as broad band at ~580 and ~800 cm^{-1} from the polymeric surface vanadia species, whereas V–O–support bond stretches at 900 cm^{-1} on the supported V_2O_5/Al_2O_3 catalyst [18]. The corresponding Raman spectra for the dehydrated supported V_2O_5/Nb_2O_5 catalysts have previously been reported and the surface VO_4 species on Nb_2O_5 exhibit the surface V=O vibration at 1035 cm^{-1} at monolayer surface coverage [11].

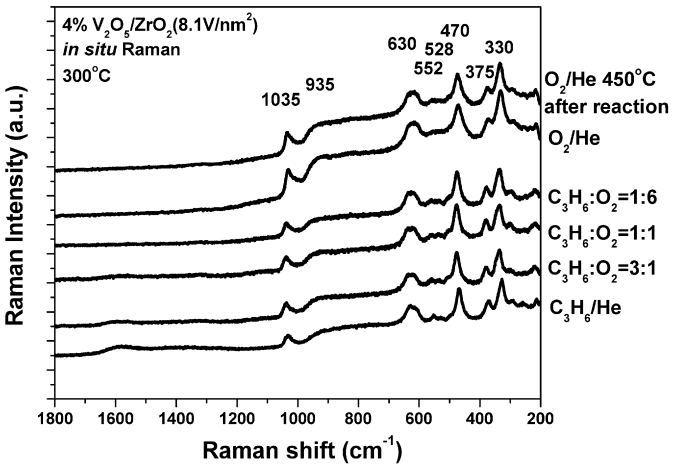

Fig. 1. *In situ* Raman spectra of supported V_2O_5/ZrO_2 at 300 °C under various environmental conditions. The strong Raman bands between 200 and 700 cm^{-1} are from the ZrO_2 (monoclinic) support.

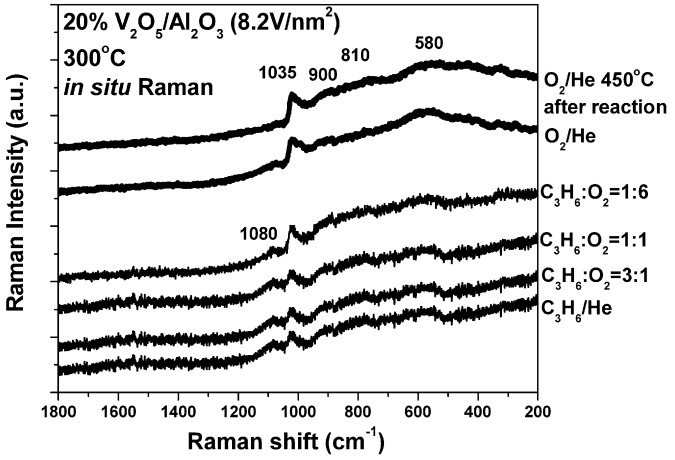

Fig. 2. *In situ* Raman spectra of supported V_2O_5/Al_2O_3 at 300 °C under various environmental conditions.

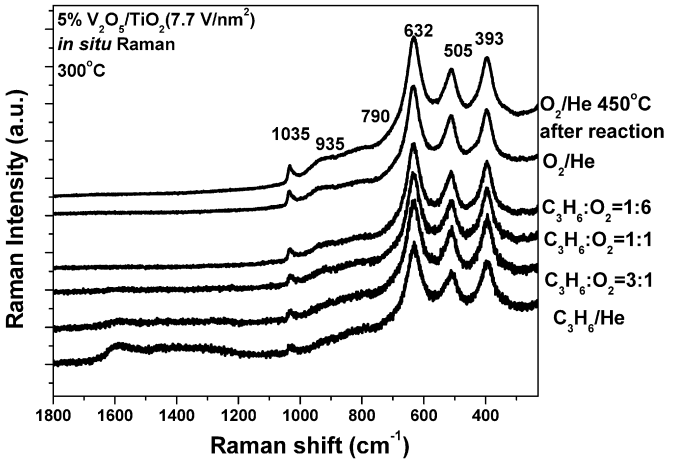

Fig. 3. *In situ* Raman spectra of supported V_2O_5/TiO_2 at 300 °C under various environmental conditions. The strong Raman bands between 300 and 800 cm^{-1} are from the TiO_2 (anatase) support.

The monolayer supported vanadia catalysts on the ZrO_2, Al_2O_3, TiO_2 and Nb_2O_5 supports have been shown to primarily consist

Table 2
Relative extents of reduction and edge energy, Eg, values of supported vanadia catalysts (relative to the oxidized catalysts) during propylene oxidation/reduction from UV–vis DRS

Catalysts	Reduction at 300 °C (%)				Eg (eV), O_2/He	ΔEg			
	C_3H_6/O_2 ratio			C_3H_6/He 2.96%		C_3H_6/O_2 ratio			C_3H_6/He 2.96%
	1:6	1:1	3:1			1:6	1:1	3:1	
1VSi	0.0	0.0	0.0	0.0	3.51	0.00	0.00	0.00	0.00
5VSi	0.0	0.0	0.0	0.0	3.51	0.00	0.00	0.00	0.00
8VSi	0.0	0.0	0.0	0.0	3.48	0.00	0.00	0.00	0.00
1VAl	0.0	0.0	0.0	0.4	3.77	0.00	0.00	0.00	0.00
5VAl	1.2	1.8	5.7	7.5	3.60	0.00	0.00	0.00	0.00
20VAl	5.7	11.2	15.5	18.3	3.03	0.01	0.02	0.08	0.09
1VZr	3.2	5.5	5.9	8.3	3.46	0.00	0.00	0.01	0.01
3VZr	5.4	9.6	10.3	20.2	3.26	0.00	0.02	0.08	0.12
4VZr	15.3	22.8	39.2	64.6	3.10	0.03	0.10	0.12	0.15

of polymeric surface VO_4 species and only minor amounts of isolated surface VO_4 species under dehydrated conditions [19]. For the supported V_2O_5/SiO_2 catalysts, however, the dehydrated Raman spectra reveal only the presence of isolated surface VO_4 species with the terminal V=O and bridging V–O–Si bands at ~1038 and 905 cm^{-1}, respectively, and the absence of bridging V–O–V bands in the 500–800 cm^{-1} region [19,20]. The Raman spectra for the dehydrated supported V_2O_5/SiO_2 catalysts have previously been reported [19,20]. The maximum dispersion of vanadia on SiO_2, where V_2O_5 NPs are not present, corresponds to ~2.7 V/nm^2. The lower dispersion capacity of the SiO_2 support is related to the lower reactivity of the SiO_2 surface hydroxyls [21].

3.2.2. *In situ* Raman spectroscopy during propylene oxidation (300 °C)

The *in situ* Raman spectra of the monolayer supported V_2O_5/ZrO_2, V_2O_5/Al_2O_3 and V_2O_5/TiO_2 catalysts during propylene oxidation reaction at 300 °C are presented in Figs. 1–3, respectively. The surface VO_4 species partially reduce in the propylene oxidation environment, especially with increasing C_3H_6/O_2 ratio, as reflected in the decrease of their Raman bands at ~1035 cm^{-1} [19,22]. This trend was also found for monolayer supported V_2O_5/Nb_2O_5 catalysts [23], but not for supported V_2O_5/SiO_2 that did not reduce during propylene oxidation [20]. The qualitative trends are that the reduction extent of the surface VO_4 species depends on both the oxide support and surface vanadia coverage. Additional weak Raman bands at ~1400 and ~1600 cm^{-1} from minor amounts of poly-aromatic carbon deposits are also present during propylene oxidation when stoichiometric excess C_3H_6 is present ($O_2/C_3H_6 < 1$) [23]. The minor amount of surface carbon residue is readily combusted in flowing O_2/He at 450 °C and the supported vanadia catalysts readily return to their initial fully oxidized states.

3.3. *In situ* UV–vis DRS spectroscopy

3.3.1. *In situ* UV–vis DRS of dehydrated catalysts (300 °C)

The UV–vis DRS edge energy, Eg, provides information about the extent of polymerization of surface vanadia species on oxide supports [13,19]. The Eg values for the fully oxidized and dehydrated supported vanadium oxide catalysts are given in Table 2. For the dehydrated supported V_2O_5/SiO_2 catalysts, the Eg values are ~3.48–3.51 eV that correspond to the Eg value of isolated surface VO_4 species [22]. For both dehydrated supported V_2O_5/Al_2O_3 and V_2O_5/ZrO_2 catalysts, the Eg values decrease from 3.77/3.46 to 3.03/3.10 eV, respectively, with increasing vanadia surface density in the sub-monolayer region. This trend reflects the progressive polymerization of the surface VO_4 species with surface coverage on these supports [13,19]. These UV–vis DRS Eg values reveal that isolated surface VO_4 species predominate at low vanadia surface density and polymeric surface vanadia species are dominant at monolayer surface coverage for the dehydrated supported V_2O_5/Al_2O_3 and V_2O_5/ZrO_2 catalysts. Thus, with the exception of supported V_2O_5/SiO_2 where only isolated surface VO_4 species are present, the extent of polymerization of the dehydrated surface VO_4 species on oxide supports depends on both the specific oxide support and surface coverage in the sub-monolayer region. The UV–vis spectra for the supported V_2O_5/TiO_2 and V_2O_5/Nb_2O_5 catalyst were not measured because of the strong UV–vis absorbance by the TiO_2 and Nb_2O_5 supports in the region of interest, but the same Raman shifts with surface vanadia coverage suggest that the same surface VO_4 polymerization process also takes place on these oxide supports [19,22,23]. The *in situ* UV–vis spectra demonstrate that isolated surface VO_4 species predominate at low surface vanadia coverage on all supports and polymeric surface VO_4 species are dominant as monolayer surface coverage is approached.

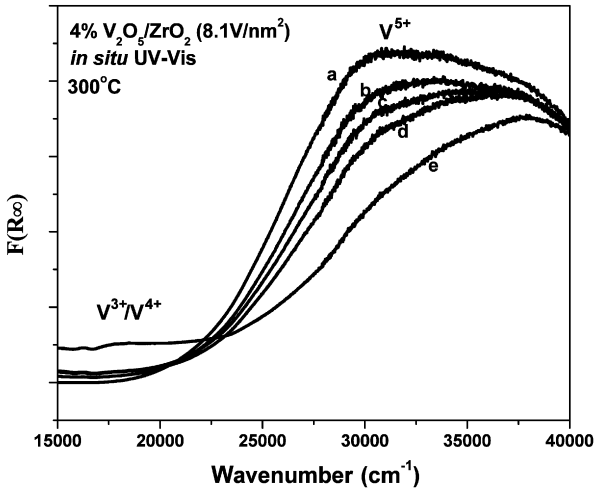

Fig. 4. *In situ* UV–vis DRS spectra of supported 4% V_2O_5/ZrO_2 at 300 °C under various environmental conditions: (a) O_2/He; (b) $C_3H_6:O_2 = 1:6$; (c) $C_3H_6:O_2 = 1:1$; (d) $C_3H_6:O_2 = 3:1$; and (e) C_3H_6/He.

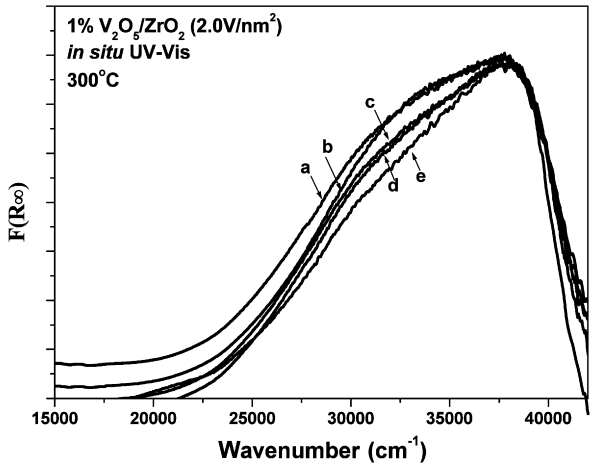

Fig. 5. *In situ* UV–vis DRS spectra of supported 1% V_2O_5/ZrO_2 at 300 °C under various environmental conditions: (a) O_2/He; (b) $C_3H_6:O_2 = 1:6$; (c) $C_3H_6:O_2 = 1:1$; (d) $C_3H_6:O_2 = 3:1$; and (e) C_3H_6/He.

3.3.2. *In situ* UV–vis DRS during propylene oxidation (300 °C)

The *in situ* UV–vis DRS of the supported 4% V_2O_5/ZrO_2 (8.1 V/nm^2) and 1% V_2O_5/ZrO_2 (2.0 V/nm^2) catalysts during propylene oxidation at 300 °C are presented in Figs. 4 and 5, respectively. The oxygen ligand to metal charge transfer (LMCT) band of the surface V(V) species occurs above 22,000 cm^{-1} and the d–d transitions of the surface V(IV)/V(III) cations appear below 22,000 cm^{-1} [13].

For the supported 4% V_2O_5/ZrO_2 catalyst, the surface V(V) cations progressively reduce to surface V(IV)/V(III) cations with increasing C_3H_6/O_2 ratios. The supported 1% V_2O_5/ZrO_2 catalyst, however, only exhibits minor reduction in the intensity of the LMCT of the surface V(V) cations and minor increase in the intensity of the d–d band under comparable reactive environments (see Fig. 5). Thus, the polymeric surface VO_4 species become more extensively reduced during propylene oxidation than isolated surface VO_4 species.

The relative extent of reduction under the different reactive environments for the supported V_2O_5/ZrO_2, V_2O_5/Al_2O_3 and V_2O_5/SiO_2 catalysts are determined from the reduction of the LMCT band of the V(V) cation and are listed in Table 2. The supported V_2O_5/SiO_2 catalysts (0.2–2.7 V/nm^2), which exclusively consist of isolated surface VO_4 species [19,22], however, does not undergo any reduction during propylene oxidation. The supported 1% V_2O_5/Al_2O_3 catalyst (0.3 V/nm^2) that also exclusively contains isolated surface VO_4 species [19,22] also does not become reduced during propylene oxidation. The minor reduction of the supported 1% V_2O_5/ZrO_2 catalyst (2.0 V/nm^2) is related to the presence of some polymeric surface VO_4 species in this higher vanadia surface density sample [19,22]. At monolayer surface vanadia coverage (~8 V/nm^2), the polymeric surface VO_4 species are more reduced on the ZrO_2 support than the Al_2O_3 support during propylene oxidation. Similar conclusions were made above from the *in situ* Raman measurements about the reduction extent of the supported V_2O_5/TiO_2 and V_2O_5/Nb_2O_5 catalysts during propylene oxidation reaction conditions.

The *in situ* UV–vis DRS data reveal that the surface VO_4 species (i) are predominantly oxidized during propylene oxidation at 300 °C, especially under typical oxidizing conditions (O_2/C_3H_6 ratio $\gg$ 1), (ii) the extent of reduction strongly depends on the specific oxide support at the same coverage (V_2O_5/ZrO_2 > V_2O_5/Al_2O_3 > V_2O_5/SiO_2), (iii) the extent of reduction increases with vanadia surface density and (iv) increasing the partial pressure of molecular O_2 decreases the extent of reduction for highly reducing reaction environments (O_2/C_3H_6 < 1).

3.4. Propylene oxidation catalytic studies

The catalytic performance for the selective oxidation of propylene over the supported vanadium oxide catalysts are presented in Tables 3 and 4 as a function of the oxide support, vanadia surface density in the sub-monolayer region and the C_3H_6/O_2 ratio.

3.4.1. Reaction selectivity

The acrolein selectivity varies from ~35 to 90% for the different supported vanadia catalysts. Among the various supported vanadia catalysts, only the supported V_2O_5/Nb_2O_5 catalyst yields acrolein selectivity in the 90% range. For low surface vanadia coverage (~1–2 V/nm^2), where isolated surface VO_4 species predominate, comparable acrolein selectivity is found for all the supported vanadia catalysts. The acrolein selectivity is not a function of vanadia surface density for supported V_2O_5/ZrO_2, V_2O_5/TiO_2 and V_2O_5/SiO_2, but the acrolein selectivity does increase with vanadia surface density for the supported V_2O_5/Nb_2O_5 and V_2O_5/Al_2O_3 catalysts. The relatively constant acrolein selectivity with surface vanadia coverage on supported V_2O_5/ZrO_2 and V_2O_5/TiO_2 catalysts suggests that isolated and polymeric surface VO_4 species intrinsically exhibit the same acrolein selectivity during propylene oxidation. The acrolein selectivity was also relatively independent for different C_3H_6/O_2 ratios. In addition to acrolein, the supported V_2O_5/Nb_2O_5 and V_2O_5/SiO_2 catalysts also produce significant amounts of acetone.

Table 3
Catalytic results of propylene oxidation to acrolein at 300 °C ($C_3H_6/O_2/He = 1:4:5$, total flow rate 50 ml/min)

Support	Catalyst	TOF[a] (10^{-3} s^{-1}) 300 °C	Selectivity[b] (%)					
			Acr	Ace	AA	CO_2	CO	Others
ZrO_2	1VZr	6.1	44.7	3.1	8.0	19.6	24.6	tr
	3VZr	11	35.8	2.0	5.7	26.7	25.8	4.0
	4VZr	24	38.8	0.7	3.1	13.1	33.1	11.2
TiO_2	1VTi	3.1	49.2	1.1	1.9	14.0	33.8	0.0
	2VTi	6.0	43.2	0.8	0.8	25.6	29.6	tr
	3VTi	12	50.4	0.6	3.3	10.1	35.2	0.4
	5VTi	20	46.7	1.8	2.1	21.5	26.7	1.2
Nb_2O_5	1VNb	1.0	51.6	21.8	3.8	7.2	1.1	14.5
	3VNb	2.1	71.9	14.2	3.9	2.8	0.0	7.2
	5VNb	3.2	75.3	14.1	2.9	2.1	0.0	5.6
	7VNb	4.7	90.7	7.3	0.0	0.0	0.9	1.1
Al_2O_3	5VAl	0.35	58.8	3.2	5.2	13.6	19.2	0.0
	10VAl	0.42	65.4	5.9	4.1	10.7	13.9	0.0
	20VAl	1.3	74.4	0.7	0.9	10.9	12.8	0.3
SiO_2	1VSi	0.5	51.9	43.9	2.2	0.1	0.7	1.2
	5VSi	0.5	48.9	45.1	5.7	0.0	0.3	0.0
	8VSi	0.6	48.2	49.7	0.3	0.0	1.3	0.5

[a] TOF based on acrolein formation.
[b] Acr: acrolein; Ace: acetone; AA: acrylic acid; Others: mainly two carbon products including acetaldehyde and ethylene, etc.

Table 4
Effect of O_2 and propylene partial pressures on the TOF and selectivity values for propylene oxidation to acrolein over supported vanadium oxide catalysts with monolayer surface VO_4 coverage, with the exception of SiO_2 where monolayer coverage is not achievable

Catalysts	Gas condition C_3H_6:O_2	TOF[a] 10^{-3} s^{-1}	Selectivity[b] (%)					
			Acr	Ace	AA	CO	CO_2	Others
4VZr	1:4	24	39	1	3	33	13	11
	1:2	19	29	Trace	0	38	25	8
	1:1	16	30	Trace	0	29	29	12
5VTi	1:4	20	47	2	2	27	21	1
	1:2	18	42	5	1	28	23	1
	1:1	15	44	3	1	30	22	0
7VNb	1:4	4.7	91	7	0	1	0	1
	1:2	4.4	88	8	0	2	0	2
	1:1	3.8	90	7	0	2	0	1
20VAl	1:4	1.3	74	1	1	13	11	0
	1:2	0.98	72	3	2	12	8	3
	1:1	0.88	74	4	0	12	9	1
5VSi	1:4	0.50	49	45	6	0	0	0
	1:2	0.50	48	46	6	0	0	0
	1:1	0.30	48	47	5	0	0	0

[a] TOF based on acrolein formation.
[b] Acr: acrolein; Ace: acetone; AA: acrylic acid; Others: mainly two carbon products including acetaldehyde and ethylene, etc.

3.4.2. Reaction activity

The acrolein TOF (TOF is defined as acrolein formed per exposed surface vanadia site per second) varies by more than a factor of 10^2 at 300 °C with the specific oxide support both at low coverage and monolayer coverage. The supported V_2O_5/ZrO_2 and V_2O_5/TiO_2 catalysts are the most active while the supported V_2O_5/SiO_2 catalyst system displays the lowest activity. The acrolein TOF reactivity trend of V_2O_5/ZrO_2 > V_2O_5/TiO_2 > V_2O_5/Nb_2O_5 > V_2O_5/Al_2O_3 > V_2O_5/SiO_2 reflects the pronounced effect of the specific oxide support upon the TOF values. The acrolein TOF also increases by a factor of 4–6 with surface vanadia coverage for the supported vanadia catalysts and is relatively constant for the supported V_2O_5/SiO_2 catalysts with surface coverage. Furthermore, for a given support vanadia catalyst system, increasing the O_2/C_3H_6

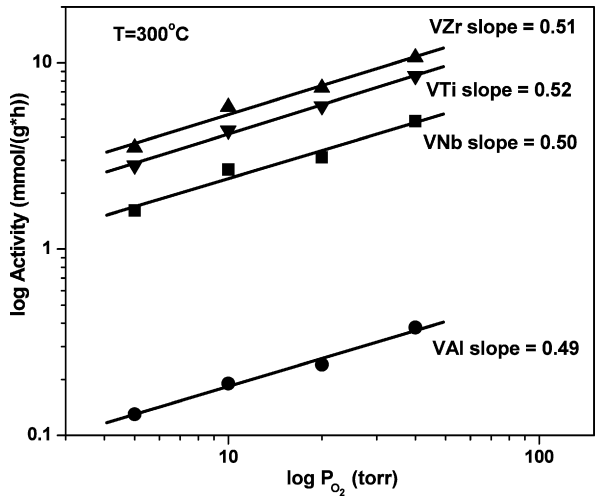

Fig. 6. Dependence of kinetics for propylene oxidation to acrolein on the gas phase molecular O_2 partial pressure at 300 °C.

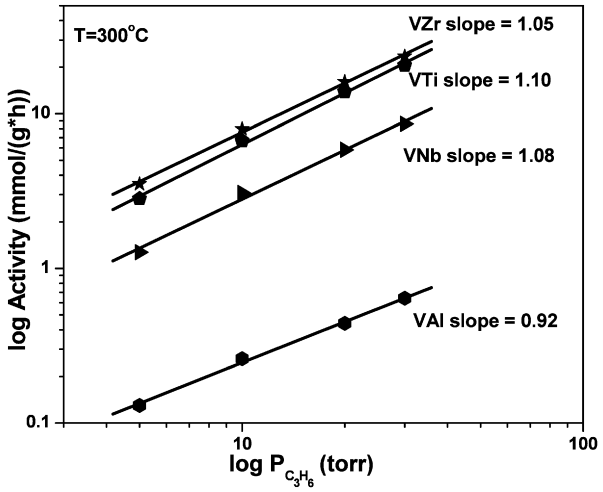

Fig. 7. Dependence of kinetic for propylene oxidation to acrolein on the gas phase C_3H_6 partial pressure at 300 °C.

ratio leads to a factor of ~1.5 increase in acrolein TOF for the supported vanadium oxide catalysts (see Table 4). This latter observation suggests that fully oxidized V(V) surface VO_4 species are more efficient than reduced V(IV/III) for propylene oxidation to acrolein.

3.4.3. Reaction kinetics and number of participating catalytic active sites

The kinetics of propylene oxidation to acrolein follows 1st- and ½-order in the partial pressures of C_3H_6 and O_2, respectively, as shown in Figs. 6 and 7. With the exception of the supported V_2O_5/SiO_2 catalyst system, the supported vanadia catalysts exhibit a continuous increase in acrolein TOF with surface VO_4 coverage in the sub-monolayer region. An increase in TOF with surface vanadia coverage was previously not observed for oxidative dehydrogenation reactions over supported vanadium oxide catalysts (e.g., CH_3OH to H_2CO [16], C_2H_6 to C_2H_4 [24], C_3H_8 to C_3H_6 [13,19]). The current increase in acrolein TOF with surface vanadia coverage suggests that more than one surface VO_4 site may be involved in the rate-determining-step (rds) of propylene oxidation to acrolein. It is possible to determine the dependence of the propylene oxidation reaction on the number of participating surface VO_4 sites since the surface vanadia coverage on the oxide supports can be controlled below the sub-monolayer region.

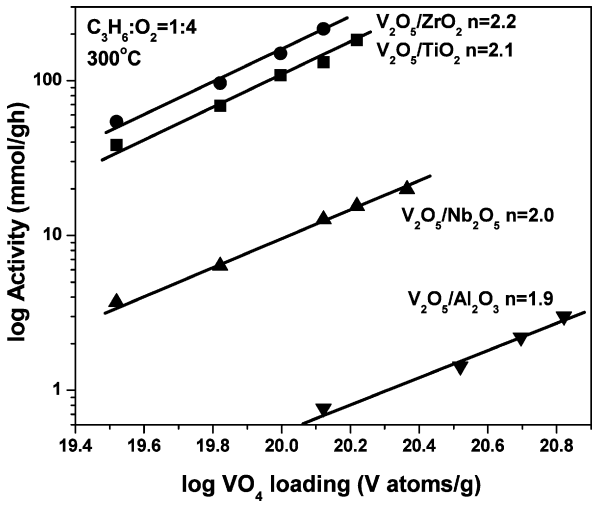

Fig. 8. Plot of log activity (mmol/g h) vs log Ns (V/g) for $T = 300$ °C and $C_3H_6{:}O_2 = 1{:}4$.

For supported vanadium oxide catalysts, the number of catalytic active surface VO_4 sites/g increases linearly with vanadia loading in the sub-monolayer region where vanadia is 100% dispersed on the supports. This linear relationship allows for the quantitative determination of the number of surface catalytic active sites involved in the rate-determining-step of propylene oxidation to acrolein since. Thus, the kinetic expression for the rate of propylene oxidation to acrolein can be expressed as:

$$r = k'[C_3H_6]^1[O_2]^{0.5}[Ns]^n, \quad (1)$$

in which r represents the rate of reaction of propylene oxidation to acrolein (mmol acrolein/(g h)), k' is the product of the equilibrium adsorption constant (K_{ads}) and the Arrhenius rate constant (k_{rds}), Ns is the number of surface vanadia sites/g, and n represents the number of catalytic sites involved in the rate-determining-step of propylene oxidation to acrolein. For constant partial pressures of the reactants, temperature, and flow rates, Eq. (1) can be further simplified as

$$r = k''[Ns]^n, \quad (2)$$

in which k'' includes all the constant parameters (k', $[C_3H_6]^1$ and $[O_2]^{0.5}$). The exponent n can be readily determined from the slope of the plot of log [rate (mmol acrolein/(g h))] vs log[Ns (V/g)]. Such plots are shown in Fig. 8 for the supported V_2O_5/ZrO_2, V_2O_5/TiO_2, V_2O_5/Nb_2O_5, and V_2O_5/Al_2O_3 catalysts. For propylene oxidation to acrolein over the supported vanadia catalysts, such plots yield slopes of $n = 1.9$–2.2 for the various supported vanadia catalysts. Interestingly, comparable slopes are obtained for catalysts that have constant acrolein selectivity with vanadia surface density as well as catalysts where the acrolein selectivity increases with surface vanadia coverage. A slope of ~2 suggests that two surface VO_4 sites are involved in the rds of the selective oxidation of propylene to acrolein over the supported catalysts.

4. Discussion

The combination of propylene oxidation catalytic activity/selectivity and *in situ* spectroscopic information presented above allows for the determination of the fundamental relationships between the molecular/electronic structure of the catalytic active surface vanadia sites and their catalytic performance (activity/selectivity) for propylene oxidation to acrolein.

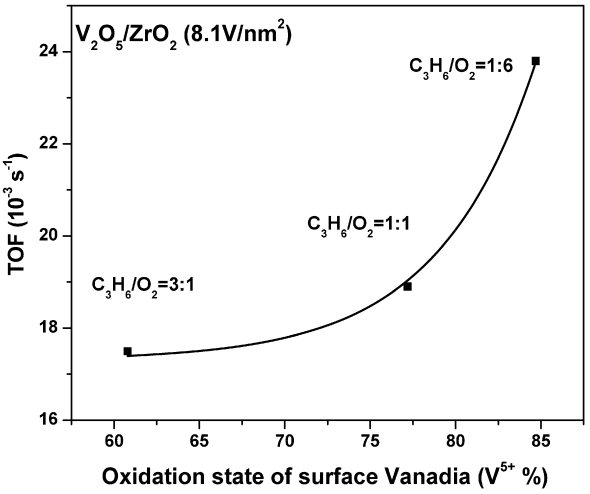

Fig. 9. Relationship between oxidation state of surface vanadia species and TOF for acrolein formation over supported V_2O_5/ZrO_2 at 300 °C.

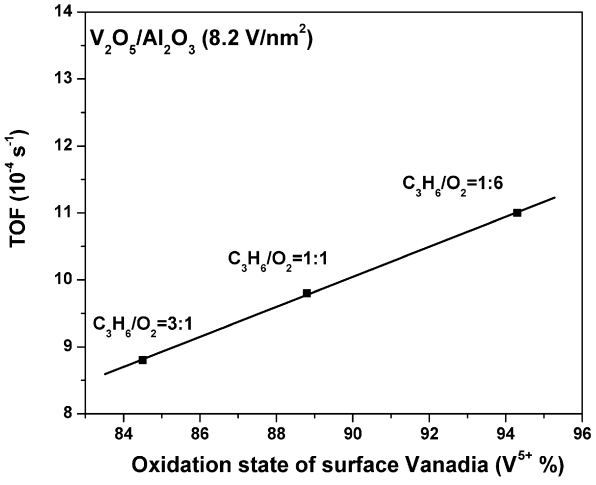

Fig. 10. Relationship between oxidation state of surface vanadia and TOF for acrolein formation over supported V_2O_5/Al_2O_3 at 300 °C.

4.1. Nature of catalytic active site

The surface VO_4 species are the catalytic active sites for propylene oxidation to acrolein since the vanadium-free oxide supports do not selectively oxidize propylene and the acrolein TOF also increases with increasing surface vanadia coverage. The *in situ* Raman and UV–vis spectroscopy measurements revealed that the surface VO_4 species partially reduce during the propylene oxidation reaction at 300 °C. The extent of reduction for a given supported vanadium oxide catalyst system was found to be greater for polymeric surface VO_4 species than isolated surface VO_4 species. The extent of reduction of the surface vanadia species, however, does not alter the acrolein selectivity (see Table 4). Increasing the molecular O_2 partial pressure is found to increase both the concentration of surface V(V) sites and the acrolein TOF specific activity, as shown in Figs. 9 and 10, demonstrating that the fully oxidized surface V(V) sites are more active than reduced surface vanadia sites for propylene oxidation on a given oxide support. Note, however, that this increase is less than a factor of 1.5 over the region investigated since the majority of the surface VO_4 sites are present as V(V) under the reaction conditions.

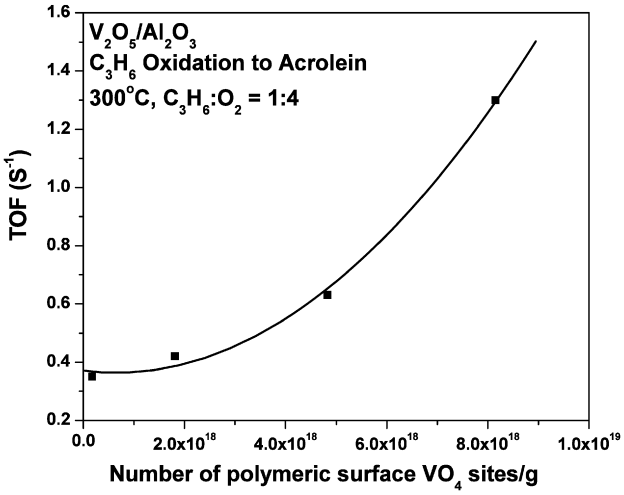

Fig. 11. Relationship between propylene oxidation to acrolein TOF and percent polymeric surface vanadia species over supported V_2O_5/Al_2O_3 catalysts at 300 °C. (Percent polymer obtained from Ref. [19].)

4.2. Surface VO_4 coverage

As is well established in the literature [19,22] and shown above with the UV–vis DRS data (see Table 2), both isolated and polymeric surface VO_4 species exist on the oxide supports and, with the exception of supported V_2O_5/SiO_2, the ratio of polymeric/monomeric species increases with surface vanadia coverage. For propylene oxidation, the acrolein selectivity is found to be independent of surface vanadia coverage or surface VO_4 polymer/monomer ratio for the supported V_2O_5/ZrO_2 and V_2O_5/TiO_2 catalysts. This finding suggests that the acrolein selectivity is comparable for surface VO_4 monomeric and polymeric species. For supported V_2O_5/Nb_2O_5 and V_2O_5/Al_2O_3, however, the acrolein selectivity increases with surface vanadia coverage or surface VO_4 polymer/monomer ratio. This finding suggests that a factor besides the surface VO_4 polymer/monomer ratio is contributing to the enhanced selectivity with increasing surface vanadia coverage. Both the Al_2O_3 and Nb_2O_5 supports are the most acidic oxide supports in this series and coverage of these exposed acid sites by the surface VO_4 overlayer most probably is responsible for enhancing their acrolein selectivity with increasing surface vanadia coverage.

The TOF values for propylene oxidation to acrolein increase by a factor of ~5 with increasing surface vanadia coverage or vanadia surface density, even for those catalytic systems that exhibit constant acrolein selectivity with surface vanadia coverage. This increase in acrolein TOF could possibly be interpreted as polymeric surface VO_4 species being more active than isolated surface VO_4 species. The number of polymeric and monomeric surface VO_4 species present in the supported V_2O_5/Al_2O_3 and V_2O_5/ZrO_2 are provided from the UV–vis DRS measurements (see Table 2) [19,22]. The plots of propylene oxidation to acrolein TOF vs number of polymeric VO_4 sites in these two supported vanadium oxide catalysts (sites/g) are shown in Figs. 11 and 12 and do not result in a linear relationship between these two parameters. At intermediate amounts of polymeric surface VO_4 species, increasing the concentration of polymeric surface VO_4 species has a minor effect on TOF. At high amounts of polymeric surface VO_4 species concentrations, increasing the concentration polymeric surface VO_4 species gives rise to an exponential-type relationship. The absence of a linear relationship between the acrolein TOF and number of polymeric surface VO_4 sites in the catalysts, especially at intermediate concentrations, demonstrates that polymeric surface VO_4 species are not responsible for the increase in propylene oxidation to acrolein TOF with surface vanadia coverage. This is also born

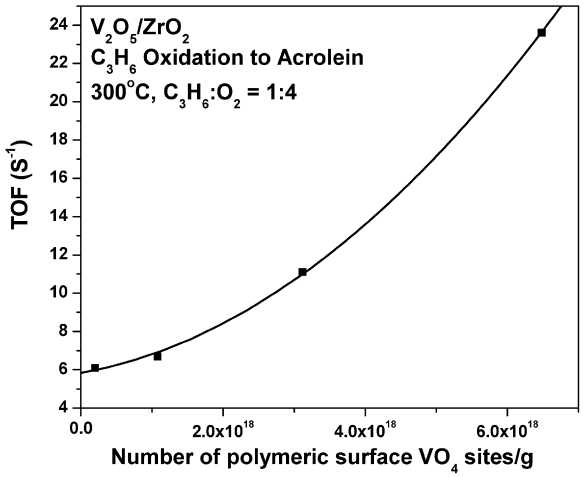

Fig. 12. Relationship between propylene oxidation to acrolein TOF and percent polymeric surface vanadia species over supported V_2O_5/ZrO_2 catalysts at 300 °C. (Percent polymer obtained from Ref. [19].)

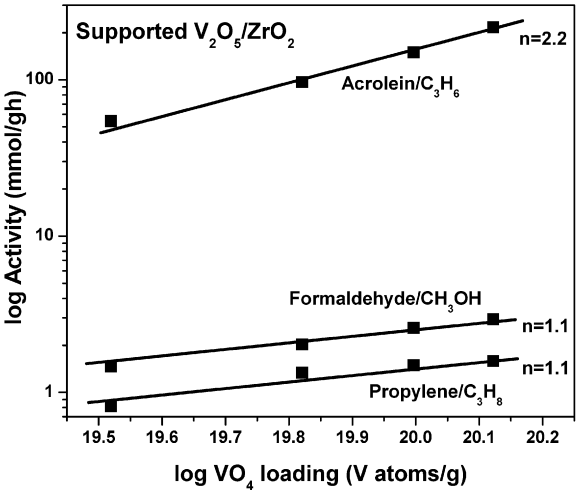

Fig. 13. The number of participating catalytic active sites in the rate-determining-step for oxidation of different molecules over supported V_2O_5/ZrO_2 catalysts is provided by the slope of log activity vs log V atoms/g.

out by many other oxidation reactions over supported vanadia catalysts that exhibit the same TOF for isolated and polymeric surface VO_4 species [13,16,19–32].

The major difference between propylene oxidation and the above mentioned oxidation reactions over supported vanadia catalysts is that propylene oxidation to acrolein is a $4e^-$ reaction involving two surface VO_4 sites while the $2e^-$ reactions for the oxidative dehydrogenation (ODH) reactions of propane to propylene and CH_3OH to HCHO only involve one surface VO_4 site. This is shown in Fig. 13 where the number of sites involved in the rds is determined from the plots of activity vs V/g present in the catalysts for these oxidation reactions as a function of surface vanadia coverage. Thus, the increase in acrolein TOF with surface vanadia coverage is strictly a consequence of the requirement of two surface VO_4 sites for the more complex propylene oxidation to acrolein reaction. A similar finding was earlier made for the even more complex oxidation of *n*-butane to maleic anhydride, an $8e^-$ reaction, over supported vanadia catalysts [33].

4.3. Specific oxide support

Although increasing the surface vanadium oxide coverage generally increases the acrolein TOF by a factor ~5, the acrolein TOF

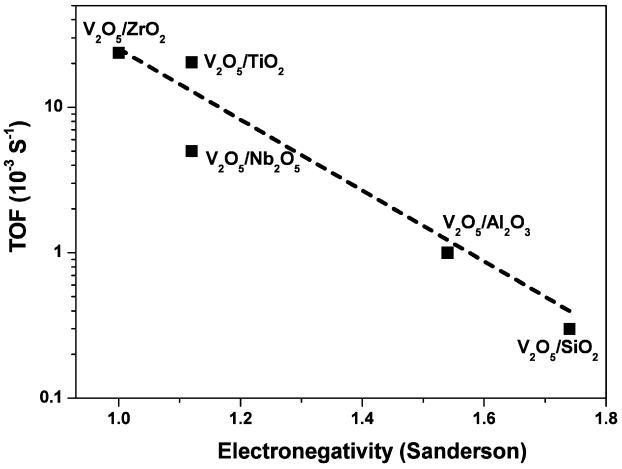

Fig. 14. Relationship between propylene oxidation to acrolein TOF and electronegativity of the oxide support cation over monolayer supported vanadium oxide catalysts, with the exception of the supported V_2O_5/SiO_2 catalyst that does not possess monolayer coverage.

changes by a factor of $\sim 10^1$–10^2 with the specific oxide support. At low surface vanadia coverage (~1–2 V/nm^2), the surface VO_4 species are almost exclusively isolated and the acrolein TOF varies by a factor of ~20 with oxide support. At monolayer surface vanadia coverage (~8 V/nm^2), the surface VO_4 species are almost entirely present as polymeric species and the acrolein TOF also varies by a factor of ~20. The overall support effect further increase by a factor of ~50 when the maximum dispersed supported V_2O_5/SiO_2 catalyst is also taken into consideration. Thus, the specific oxide support has the most pronounced effect on the propylene oxidation to acrolein TOF ($ZrO_2 \sim TiO_2 > Nb_2O_5 > Al_2O_3 > SiO_2$).

The propylene oxidation to acrolein TOF is found to correlate with the electronegativity of the oxide support cation as shown in Fig. 14. Decreasing the electronegativity of the oxide support cation qualitatively increases the acrolein TOF. This reflects the increased electron density on the bridging V–O–support bond and the bridging oxygen atom's availability for redox reactions such as propylene oxidation to acrolein. This also appears to result in greater reduction of the surface VO_4 sites for the more active supported vanadium oxide catalysts at the same surface VO_4 coverage during propylene oxidation to acrolein (see Table 2). Essentially the same TOF trends with the specific oxide support have also been found for other oxidation reaction over supported vanadium oxide catalysts and reflects the generality of the bridging V–O–support bond as the kinetic critical catalytic active site during oxidation reactions [13,15–18,21–24,26,29,30,34]. This suggests the universal effect of the oxide support on the activity of supported vanadium oxide catalysts as well as other supported metal oxide catalysts (MoO_3 [35], CrO_3 [36], Re_2O_7 [37], WO_3 [38], Nb_2O_5 [39,40] and Ta_2O_5 [39,40]).

5. Conclusions

The *in situ* Raman and UV–vis spectroscopic studies of the supported vanadia catalysts during propylene selective oxidation to acrolein indicate that the catalytic active surface VO_4 sites become partially reduced under reaction conditions. Combination of the catalytic activity with *in situ* spectroscopic information reveals that fully oxidized surface V(V) sites are the catalytic active sites. The selective oxidation of propylene to acrolein was found to involve two surface VO_4 sites in the rds of this $4e^-$ redox reaction. Although increasing the surface vanadia coverage increases the propylene oxidation to acrolein TOF by a factor of ~5, changing the specific oxide support has a much more pronounced ef-

fect and varies the acrolein TOF by a factor $\sim 10^1$–10^2. This enhancement in catalytic activity is attributed to the electronegativity of the oxide support cation that controls the electron density on the bridging V–O–support bond available for redox reactions.

Acknowledgment

Financial support of this research by the U.S. Department of Energy-Basic Energy Sciences, Grant DE-FG02-93ER14350 is gratefully acknowledged.

References

[1] D.B. Dadyburjor, S.S. Jewur, E. Ruckenstein, Catal. Rev. 19 (1979) 293.
[2] R.K. Grasselli, in: G. Ertl, H. Knoezinger, J. Weitkamp (Eds.), Handbook of Heterogeneous Catalysis, vol. V, VCH Verlagsgesellschaft mbH, Weinheim, 1997, p. 2303.
[3] C.R. Adams, T.J. Jennings, J. Catal. 2 (1962) 63.
[4] F. Cavani, F. Trifiro, Stud. Surf. Sci. Catal. 110 (1997) 19.
[5] K. Dosumov, S.A. Tungatarova, K.K. Kuzembaev, B.K. Masalimova, Izvestiya Natsional'noi Akademii Nauk Respubliki Kazakhstan, Seriya Khimicheskaya 5 (2004) 70.
[6] Y. Kim, W. Ueda, Y. Morooka, Chem. Lett. 4 (1989) 531.
[7] T. Tanaka, M. Ooe, T. Funabiki, S. Yoshida, J. Chem. Soc. Faraday Trans. 82 (1986) 35.
[8] F. Amano, T. Tanaka, Jpn. Chem. Lett. 35 (2006) 468.
[9] M. Li, J. Shen, J. Catal. 205 (2002) 248.
[10] H. Mori, H. Ueno, N. Mizuno, H. Yahiro, M. Iwamoto, Chem. Lett. 228 (1990) 2289.
[11] C. Zhao, I. Wachs, J. Phys. Chem. C (2008), in press.
[12] B.M. Weckhuysen, I.E. Wach, Catal. Today 49 (1999) 441.
[13] X. Gao, I. Wachs, J. Catal. 209 (2002) 43.
[14] A. Khodakov, B. Olthof, A.T. Bell, E. Iglesia, J. Catal. 181 (1999) 205.
[15] I. Wachs, Catal. Today 27 (1996) 437.
[16] G. Deo, I. Wachs, J. Catal. 146 (1994) 323.
[17] I. Wachs, B.M. Weckhuysen, Appl. Catal. A Gen. 157 (1997) 67.
[18] X. Gao, I. Wachs, Top. Catal. 18 (2002) 243.
[19] H. Tian, E.I. Ross, I. Wachs, J. Phys. Chem. B 110 (2006) 9593.
[20] C. Zhao, Ph.D. thesis, Lehigh University, Bethlehem, PA, 2007.
[21] M. De Boer, A.J. Stufkens, A. Oskam, I. Wachs, J. Chem. Soc. 17 (1996) 3259.
[22] X. Gao, I. Wachs, J. Phys. Chem. 104 (2000) 1261.
[23] C. Zhao, I. Wachs, Catal. Today 118 (2006) 332.
[24] M. Banares, M. Martinez-Huerta, X. Gao, J. Fierro, I. Wachs, Catal. Today 64 (2000) 295.
[25] S. Xie, E. Iglesia, A.T. Bell, Langmuir 16 (2000) 7162.
[26] X. Gao, M.A. Banares, I. Wachs, J. Catal. 188 (1999) 325.
[27] V. Pushkarev, V. Kovalchuk, J. D'Itri, J. Phys. Chem. B 108 (2004) 5341.
[28] M. Ristic, S. Popovic, S. Music, Mater. Lett. 58 (2004) 2658.
[29] T.C. Watling, G. Deo, K. Seshan, I. Wachs, J.A. Lercher, Catal. Today 28 (1996) 139.
[30] M.V. Martinez-Huerta, X. Gao, H. Tian, I. Wachs, J.L.G. Fierro, M.A. Banares, Catal. Today 118 (2006) 279.
[31] Z. Zhao, X. Gao, I. Wachs, J. Phys. Chem. B 107 (2003) 6333.
[32] J.P. Dunn, H. Stenger, I. Wachs, Catal. Today 51 (1999) 301.
[33] I. Wachs, J. Jehng, G. Deo, B. Weckhuysen, V. Guliants, J. Benziger, S. Sundaresan, J. Catal. 170 (1997) 75.
[34] L.J. Burcham, M. Badlani, I. Wachs, J. Catal. 203 (2001) 104.
[35] A.N. Desikan, W.M. Zhang, S.T. Oyama, J. Catal. 157 (1995) 740–748.
[36] S.M. Al-Zahrani, B.Y. Jibril, A.E. Abasaeed, Catal. Today 81 (2003) 507–516.
[37] P. Arnoldy, E.M. Van Oers, V.H.J. De Beer, J.A. Moulijn, R. Prins, Appl. Catal. 48 (1989) 241–252.
[38] I. Wachs, T. Kim, E. Ross, Catal. Today 116 (2006) 162–168.
[39] I. Wachs, Y. Chen, J. Jehng, L. Briand, T. Tanaka, Catal. Today 78 (2003) 13–24.
[40] I. Wachs, L. Briand, J. Jehng, L. Burcham, X. Gao, Catal. Today 57 (2000) 323.